IOP Publishing Measurement Science and Technology
Meas. Sci. Technol. **25** (2014) 035201 (6pp) doi:10.1088/0957-0233/25/3/035201

Three-dimensional surface phase imaging based on integrated thermo-optic swept laser

Hyo Jin Kim[1], Jaedu Cho[2], Young-Ouk Noh[3], Min-Cheol Oh[1,4], Zhongping Chen[1,2] and Chang-Seok Kim[1,5]

[1] Department of Cogno-Mechatronics Engineering, World Class University Program, Pusan National University, Busan, 609-735, Korea
[2] Department of Biomedical Engineering, University of California Irvine, CA 92612, USA
[3] Chemoptics Inc., 104-11 Monji-dong, Yusong-gu, Daejeon, 305-308, Korea
[4] School of Electrical Engineering, Pusan National University, Busan, 609-735, Korea

E-mail: ckim@pusan.ac.kr

Received 28 June 2013, revised 17 November 2013
Accepted for publication 9 December 2013
Published 30 January 2014

Abstract
We developed an optical frequency domain imaging (OFDI) system based on an integrated thermo-optic swept laser to achieve three-dimensional surface imaging. The wavelength was swept by applying a heating signal to a thermo-optic polymeric waveguide. The sub-micrometer surface profile was converted from the three-dimensional phase information of the OFDI system on various samples used as resolution targets with a step height of 120 nm.

Keywords: swept laser, polymer waveguide, optical frequency domain imaging

(Some figures may appear in colour only in the online journal)

1. Introduction

With the rapid growth of the small-component industry, there has been increased demand for cost-effective, non-contact, high-speed, high-accuracy three-dimensional (3D) surface inspection technology. Considering the build-up cost, inspection speed, submicron measurement and availability of multifunctional inspection equipment, optical surface imaging systems can provide a powerful tool for the precision components industry. There are various optical approaches to imaging 3D surface profiles. Mechanical displacements of an axial scanner can record the phase variance on a sample surface in an optical interferometer [1–3]. However, those approaches using a mechanical movement could suffer hysteresis of the mechanical translator, making them unsuitable for the increasing degree of integration of imaging systems. The alternative of employing a tunable laser source to build non-mechanical movement optical imaging systems has been extensively studied [4–6]. For the last decades, optical frequency domain imaging (OFDI), also known as swept-source optical coherence tomography, has been studied not only to avoid mechanical movement in axial scanning, but also to enhance the signal-to-noise ratio (SNR) compared to traditional optical imaging systems using a white-light-source-based time-domain process [7, 8]. OFDI is a frequency-domain-based image technique that uses a swept source and an optical interferometer. Once the swept source changes its wavelength within the designed spectral bandwidth, an OFDI system acquires spectrally resolved interference signals, which are processed by frequency domain analysis [9]. More importantly, the area-beam-type OFDI approach can be suitable for 3D surface phase imaging without any mechanical movement [10]. One of the most important issues for increasing the degree of integration of the OFDI system has to do with the swept source. Recently, a number of integrated swept sources have been demonstrated for OFDI using a resonant-mirror-based swept laser [11] and an optically pumped swept vertical-cavity surface-emitting laser [12].

However, most of these costly swept sources are intended to work at high speeds of more than 10 kHz and to

[5] Author to whom any correspondence should be addressed.

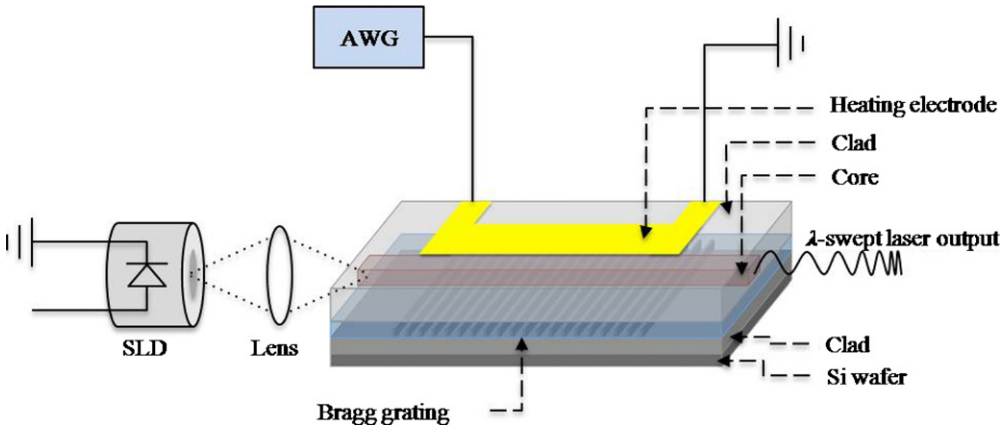

Figure 1. Schematic of the integrated thermo-optic swept laser. SLD: superluminescent diode, AWG: arbitrary waveform generator.

acquire a depth image of a multilayer structure [13]. In this study, we present an alternative novel cost-effective approach for an integrated thermo-optic swept laser to implement an integrated OFDI system for 3D surface phase imaging. This study, which employs polymeric waveguide technology, demonstrates the significant advantages of matured fabrication technology, reliable polymer material in a 1.5 μm spectral window and cost-effectiveness. However, there is still a critical disadvantage of slow response time due to the thermo-optic effect [14–16]. Nevertheless, this integrated thermo-optic swept laser can be a good choice when combined with a line-beam-type OFDI application because the line-beam-type OFDI system does not require a high repetition rate compared to the conventional point-beam-type OFDI system. The limiting factor of data acquisition in the line-beam-type OFDI is the frame rate of an array detector, such as a charge-coupled device (CCD) and a complementary metal–oxide–semiconductor (CMOS) camera (roughly a few kHz). If 1024 frames are required for 2D depth profiles, a slow repetition rate of a few Hz for the swept source can be sufficient to reconstruct the cross-sectional surface phase imaging from the array detector with thousands of pixels used in parallel. Moreover, the integrated thermo-optic swept laser can increase the degree of integration of the OFDI system. For the ultimate integration of the OFDI system on an all-in-one-chip, it can be easily expanded to integrate other polymer-waveguide-based optical components, such as the main optical interferometer, auxiliary *k*-resampling interferometer and interconnection to the optical fiber [14].

2. Experimental details

2.1. Setup for integrated thermo-optic swept laser

As shown in figure 1, the integrated thermo-optic swept laser consists of a superluminescent laser diode, an aspherical lens, Bragg grating made in a fluorinated polymer waveguide and a heating electrode on the top surface of the upper cladding. The Bragg grating waveguide was fabricated by photolithography and dry etching process. More detailed description of the fabrication process can be found in the previous paper [15]. All the components are aligned actively with a transistor outline can-type package to increase the coupling efficiency of the module and the fabrication yield. To accomplish a continuous and constant wavelength change in the swept laser output, we applied linearized power tuning to the Ti–Au heating electrode using an arbitrary function generator. To ensure stable heat distribution in the external laser cavity for a rapid-wavelength-swept output, the shape of the Ti–Au heating electrode was optimized with a polymeric tunable Bragg grating under an embedded thermoelectric cooler. Unlike the discrete tuning of the wavelength output used in wavelength division multiplexing passive optical network applications, the OFDI system requires continuous sweeping of the wavelength from the swept laser. Since the generated Joule heating energy Q is proportional to the square of the applied voltage, it gives rise to $Q(V) = \sigma V^2$, where σ is the electric conductivity of the heating electrode and V is the waveform voltage. To secure a constant wavelength change in the time domain, we applied a programmed waveform $V(t)$ that is proportional to the square root of the time as given by the following equation:

$$V(t) = \begin{pmatrix} A\sqrt{t} \\ A\sqrt{p-t} \end{pmatrix} \quad \begin{matrix} \text{when} \quad t < p/2 \\ \text{when} \quad t > p/2, \end{matrix} \tag{1}$$

where A indicates the amplitude of the electric potential, p is the period of the linearized power tuning and t is the time lapse. We have developed a thermo-optic polymer material (Exguide^{TM} LFR, Chemoptics Inc.) that has a negative thermo-optic coefficient; the launched wavelength of the laser output decreased linearly, as shown in the following equation:

$$\Delta\lambda_B = 2\frac{\Lambda_g}{m}\frac{\partial n}{\partial T}\Delta T, \tag{2}$$

where $\Delta\lambda_B$ is the range of the wavelength sweep, Λ_g is the period of the Bragg grating, m is the order of the Bragg grating, $\partial n/\partial T$ is the thermo-optic coefficient and ΔT is the range of the temperature change. Figure 2(*a*) shows that the output power spectra were flattened across the entire swept range of around 0 dBm, and the side-mode suppression ratio ranged from 45 to 50 dB. The maximum operating laser power was 5 mW at the center wavelength. The instantaneous linewidth was 0.06 nm, which was similar to the spectral resolution of an optical spectrum analyzer. Figure 2(*b*) shows the wavelength traces obtained by continuous tuning of the heating power and voltage, respectively. As indicated in

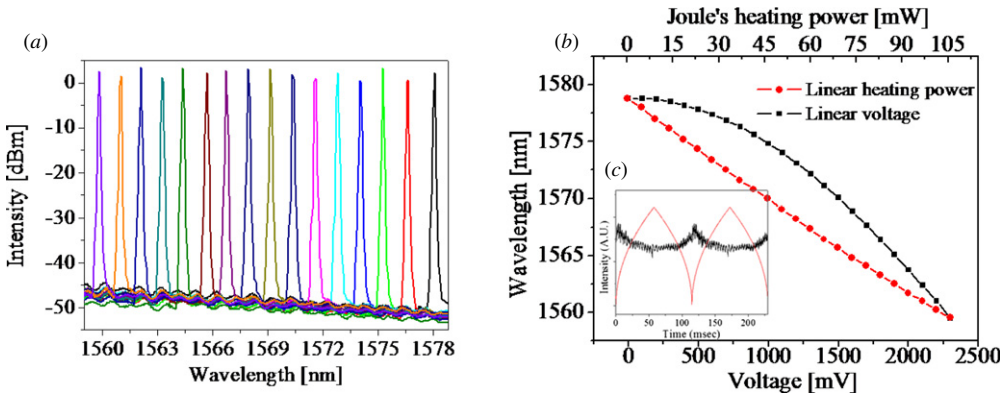

Figure 2. (*a*) Laser output spectra of discrete tuning of wavelength output, (*b*) wavelength trace of continuous tuning by applying a linearized voltage waveform and linearized heating power waveform and (*c*) temporal laser output response (black) along the linearized heating power waveform (red).

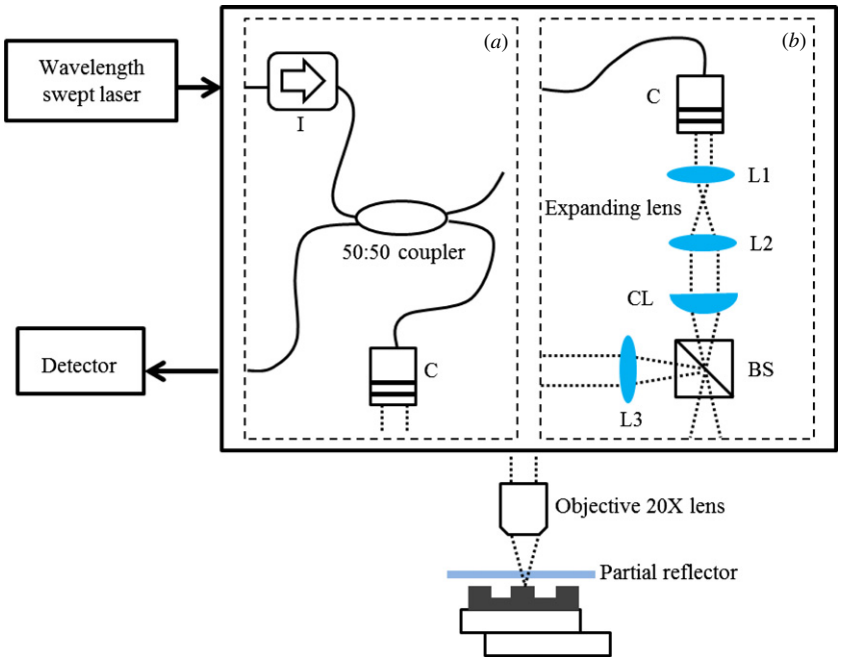

Figure 3. Setup of the OFDI system with (*a*) point-beam type, (*b*) line-beam type. I: isolator, C: collimator, CL: cylindrical lens ($f = 80$ mm), BS: beam splitter, L1: lens ($f = 30$ mm), L2: lens ($f = 100$ mm), L3: lens ($f = 50$ mm).

figure 2(*b*), the wavelength tuning slope obtained by using the linearized voltage is nonlinearly curved compared to the counterpart driven by the linearized heating power tuning. Thus, continuous and linearized wavelength sweeping should be generated according to the square of the applied voltage into this integrated thermo-optic swept laser.

2.2. Setup for the OFDI system

As shown in figure 3, the integrated thermo-optic swept laser was coupled to two types of interferometers, the point-beam type and line-beam type, in the OFDI system. These interferometers were based on a Fizeau scheme in which a common path was shared between the reference and sample arms [17–20]. This scheme shows a highly polarization-stabilized interferogram because the signal reflected from the sample and that from the partial reflector each propagate back through a common optical path [21]. Interference signals from the point-beam and line-beam common-path interferometers were received by an adjustable gain photodetector (2053-FC, New Focus, USA) and a line-scan CCD camera (SU-LDH-1.7, Goodrich Co., USA), respectively. For the point-beam type, lateral scans in the x- and y-directions were performed by two linear transverse scanning stages (M-562, Newport Co., USA). Each A-scan was performed at a repetition rate of 20 Hz, which is analogous to the rate of change of the wavelength of the swept laser. For the line-beam type, a cylindrical lens was used after the expanding lens to shape a linear beam, which removed the need for a lateral scan in the x-direction. The length and width of line-beam on the cylindrical lens focus were 6.993 mm and 23.96 μm, respectively. Because each of the 1024 pixels of the line-scan CCD camera acted as a photodetector, we could remove the B-scan from the imaging system. Only one lateral scan in the y-direction must be

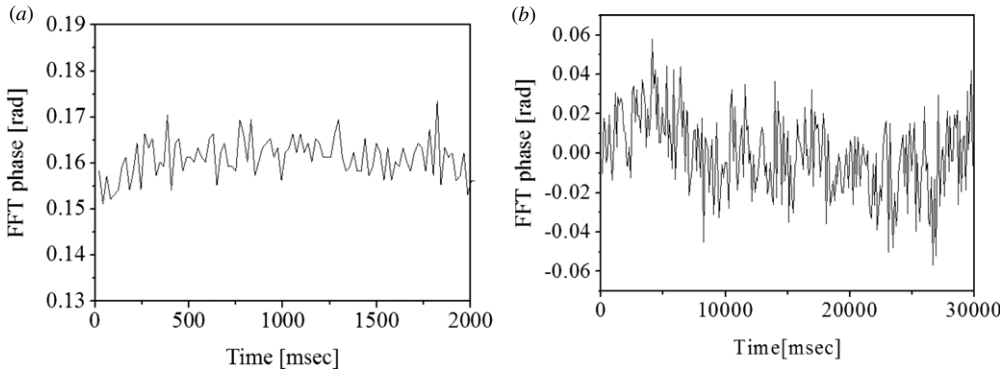

Figure 4. Standard deviation of the phase error at the same point with (*a*) the point-beam-type OFDI system and (*b*) the line-beam-type OFDI system.

performed by a linear transverse scanning stage (T-LSM200B-S, Zaber Tech., USA). The A-scan of each pixel of the line-scan CCD camera was simultaneously performed at a repetition rate of 8.736 Hz, which was determined from the rate of change of the wavelength of the swept laser and the line rate of the line-scan CCD camera. In both types of OFDI systems, the overall system operation and visualization of sampled data were performed by a customized program code written by National Instrument Co. called LabView®.

3. Image processing

To optimize the performance of the thermo-optic swept laser for OFDI system application, we maintained a constant rate of change of the laser wavelength in the time domain. However, the interference signal was a linearized function of the wavenumber k. To avoid coherence gate broadening in the frequency domain, a low-pass-filtered photodetector output signal was k-resampled using a non-uniform resampling method. Once the k-resampled signal was converted to the frequency domain by applying a fast Fourier transform algorithm, the phase information at a coherence gate was recorded as an A-scan point of a 3D surface imaging data set. The time domain interference signal $i(k)$ can be written as follows:

$$i(k) = s(k)\sqrt{E_0E_1}\cos\{2nlk + \phi\}, \tag{3}$$

where k is the wavenumber, $s(k)$ is the spectral power function of the swept bandwidth, E_0 is a reference electric field, E_1 is the sample electric field. n is an average group velocity index and l is the optical path distance (OPD) between the reference and the sample paths. The factor of 2 indicates a round trip in the reflection geometry and ϕ is the phase term of the interference signal. OFDI surface phase imaging can reduce the 2π ambiguity by using the coherence gate information. According to the Wiener–Khinchin theorem, the spectral power function of the swept bandwidth of the laser was transformed into the coherence gate function in the frequency domain. The Fourier-transformed interference signal i(z) can be written as

$$i(z) = S(z) \otimes \sqrt{E_0E_1}\delta(z \pm 2nl)\exp\{\pm \mathrm{j}\phi\}, \tag{4}$$

where z is a depth variable, $S(z)$ is the coherence gate function, δ is the Dirac delta function and j is the imaginary unit. At a certain peak of the coherence gate, the phase term ϕ contains the smaller height information, δh, for surface information within the above coherence gate:

$$\delta h = \delta\phi\lambda_0/4\pi n + \varepsilon(t), \tag{5}$$

where λ_0 is the center wavelength of the swept bandwidth, $\delta\phi$ is the phase difference of two points and $\varepsilon(t)$ is the phase error in the time domain. For the point-beam-type OFDI system, the 3D image consisted of 256 × 256 A-scans. For the line-beam one, the 3D image was $n \times N$ in size, where n is the pixel number of the line-scan CCD camera (1024) and N is the movement number for the C-scans.

4. Results

The coherence length (l_c) in the frequency domain indicates the minimum depth resolution of OPD in OFDI image, whereas the phase information at a certain OPD contains the smaller height information within sub-coherence length. The coherence length is determined by the light source. It can be written as

$$lc = \frac{2\ln 2}{\pi}\frac{\lambda_0^2}{\Delta\lambda} \tag{6}$$

where $\Delta\lambda$ and λ_0 are the spectral bandwidth and center wavelength of the light source, respectively. If δh is smaller than the coherence length, the phase readout at the OPD can be converted to relative height information of a target surface. In other words, we can reduce the 2π ambiguity of phase imaging in a coherence gate. Figure 4 illustrates the phase sensitivity of the OFDI system. The temporal phase variation was measured at an arbitrary point of the coverslip in subsequent acquisition time of more than 2000 ms. The sensitivity of the OFDI system can be characterized by the standard deviation of the phase [22]. The phase standard deviations, which are the imaging sensitivity of this system, for the point-beam- and line-beam-type systems were 0.513 nm and 1.74 nm, respectively. The phase error comes from both the thermo-optic laser itself and the common-path interferometer disturbance. The reason that the line-beam-type system was three times less stable than the point-beam type is that the free-space optical system is

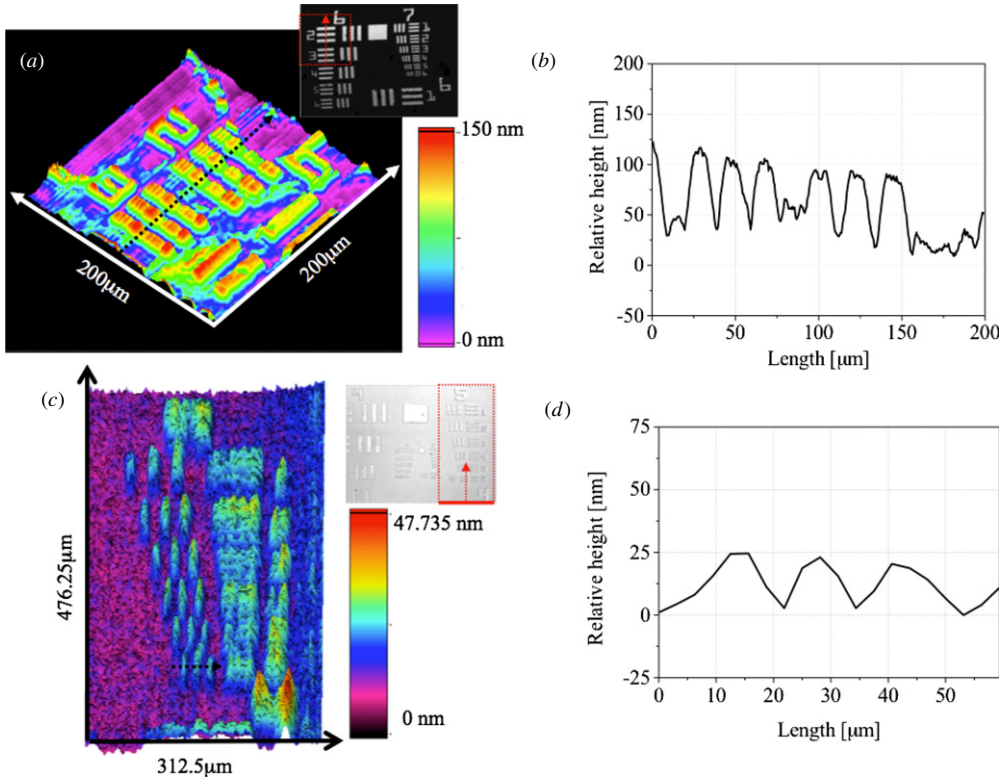

Figure 5. (*a*) 3D surface height map obtained by the point-beam-type OFDI system. Dashed arrow shows the direction of (*b*) a lateral line scan (B-scan). (*c*) A 3D surface height map obtained by the line-beam-type OFDI system. Dashed arrow in the lower center shows the direction of (*d*) a lateral line scan (B-scan). Pictures of samples are also shown in the insets of (*a*) and (*c*).

more sensitive to external vibration than the fiber-type optical system.

Figure 5 shows quantitative 3D surface images ((*a*), (*c*)) and 2D cross-sectional profiles along the lateral axis ((*b*), (*d*)). A USAF-1951 resolution target (Applied Image Inc. T-20) was visualized in the surface phase image using the developed OFDI system in figure 3. In the point-beam-type OFDI system, the region of interest (ROI) of the target was selected as group 6, elements 2 and 3, which have 6.96 μm and 6.20 μm spacing per line pair, respectively. The lateral resolution ($\sim$2.7 μm) of the point-beam-type OFDI system is determined by the laser beam spot size, which is related to the numerical aperture of the objective lens. A 3D surface image on the ROI is shown in figure 5(*a*). The 3D image size is 200 μm $\times$ 200 μm. Figure 5(*b*) shows the 2D result of a selected B-scan, which shows good conformity with the line spacing and height ($\sim$120 nm) information of the resolution target sample. The total data acquisition time was the product of the number of transverse pixels and the wavelength sweeping time, which comes to 54.6 min.

In the line-beam-type system, the ROI of the target was all elements of group 5, which have a spacing per line pair of at least 8.77 μm. A 3D surface image of the ROI is shown in figure 5(*c*). Because of the Gaussian intensity distribution of the line beam, 110 lateral pixels of the line-scan CCD camera were selected for acquiring the *x*-direction information. For *y*-directional imaging, a linear stage was moved for the C-scan along a distance of 476.25 μm with velocity 4.16 μm s^{-1}. By combining many 2D images, we could build a 3D surface phase profile with a size of 312.4 μm $\times$ 476.25 μm. Figure 5(*d*) is the 2D profile of a selected B-scan (dashed line in figure 5(*c*)). In this system, the observed *x*-direction and *y*-direction resolutions were 4.87 μm and 24.98 μm, respectively [23]. As calculated in the previous section, the *x*-direction resolution (3.125 μm) was determined by the relation between each pixel width of the line-scan CCD camera and the magnification of the optical system. On the other hand, the *y*-direction resolution (23.69 μm) was determined by the optical waist of the line beam, which is related to the focal length of the cylindrical lens and the size of the beam input to the cylindrical lens. Figure 5(*d*) shows a selected B-scanned profile, which shows that the smallest bar on group 5 was clearly resolved according to the height information ($\sim$25 nm) of the resolution target. The total data acquisition time was the product of the number of C-scan steps and the wavelength-sweeping time, which is 28.2 s. In both results, the B-scan and C-scan errors in each system were the result of the uneven group index and thickness of the partial reflector, scanning artifacts induced by a step-motor-based lateral scanning stage, and particles on the surface.

5. Conclusion

We developed an OFDI system based on an integrated thermo-optic swept laser for 3D surface phase imaging with both point-beam- and line-beam-type setups. To optimize the thermo-optic swept laser for OFDI system applications, a linearized constant rate of wavelength sweeping is achieved by applying

an arbitrary waveform to the heating electrode. The point-beam-type OFDI system showed the stability of the height measurements with the standard deviation of 0.513 nm, while the line-beam-type OFDI system enabled 116.2-fold faster data acquisition time at 2.4-fold slower laser sweeping rate than the point-beam-type OFDI system.

Even though the thermo-optic swept laser we developed has limitations on swept-bandwidth and repetition rate compared to other swept laser technologies on the shelf, those will be improved through optimized thermo-dynamic designs and polymeric waveguide fabrication techniques. The strength of the integrated thermo-optic swept laser lies in its compactness, cost-effectiveness and highly stable feature of the phase. This work will have significant impact on low-cost and compact high-precision imaging device development. Due to the stability of the phase, the thermo-optic swept laser can also be incorporated into phase-contrast microscopic applications and point-of-care biomedical imaging devices as well. In future work, the thermo-optic swept laser will be incorporated into a phase-contrast microscopic application to assess quantitative cell dynamics and subcellular microstructure with transparent cell lines.

Acknowledgments

This research was supported by the Industrial Strategic Technology Development Program (10040121) from the Ministry of Trade, Industry and Energy (MI, Korea).

References

[1] Creath K 1987 Step height measurement using two-wavelength phase-shifting interferometry *Appl. Opt.* **26** 2810
[2] Harasaki A, Schmit J and Wyant J C 2000 Improved vertical-scanning interferometry *Appl. Opt.* **39** 2107
[3] Lai C C and Hsu I J 2007 Surface profilometry with composite interferometer *Opt. Express* **15** 13949
[4] Okada K, Sakuta H, Ose T and Tsujiuchi J 1990 Separate measurements of surface shapes and refractive index inhomogeneity of an optical element using tunable-source phase shifting interferometry *Appl. Opt.* **29** 3280
[5] Suematsu M and Takeda M 1991 Wavelength-shift interferometry for distance measurements using the Fourier transform technique for fringe analysis *Appl. Opt.* **30** 4046
[6] de Groot P 2000 Measurement of transparent plates with wavelength-tuned phase shifting interferometry *Appl. Opt.* **39** 2658
[7] Leitgeb R, Hitzenberger C and Fercher A 2003 Performance of Fourier domain versus time domain optical coherence tomography *Opt. Express* **11** 889
[8] de Boer J F, Cense B, Park B H, Pierce M C, Tearney G J and Bouma B E 2003 Improved signal to noise ratio in spectral-domain compared with time-domain optical coherence tomography *Opt. Lett.* **28** 2067
[9] Yun S, Tearney G, de Boer J, Iftimia N and Bouma B 2003 High-speed optical frequency-domain imaging *Opt. Express* **11** 2953
[10] Sarunic M V, Weinberg S and Izatt J A 2006 Full-field swept-source phase microscopy *Opt. Lett.* **31** 1462
[11] Goldberg B D, Nezam S M R M, Jillella P, Bouma B E and Tearney G J 2009 Miniature swept source for point of care optical frequency domain imaging *Opt. Express* **17** 3619
[12] Grulkowski I, Liu J J, Potsaid B, Jayaraman V, Lu C D, Jiang J, Cable A E, Duker J S and Fujimoto J G 2012 Retinal, anterior segment and full eye imaging using ultrahigh speed swept source OCT with vertical-cavity surface emitting laser *Biomed. Opt. Express* **3** 2733
[13] Deck L 2002 Absolute distance measurements using FTPSI with a widely tunable IR laser *Proc. SPIE* **4778** 218
[14] Oh M C, Lee M H and Lee H J 1999 Polymeric waveguide polarization splitter with a buried birefringent polymer *IEEE Photon. Technol. Lett.* **11** 1144
[15] Noh Y O, Lee H J, Ju J J, Kim M S, Oh S H and Oh M C 2008 Continuously tunable compact lasers based on thermo-optic polymer waveguides with Bragg grating *Opt. Express* **16** 18194
[16] Son N S, Kim K J, Kim J W and Oh M C 2012 Near-infrared tunable lasers with polymer waveguide Bragg grating *Opt. Express* **20** 827
[17] Sharma U, Fried N M and Kang J U 2005 All-fiber common-path optical coherence tomography: sensitivity optimization and system analysis *IEEE J. Sel. Top. Quantum Electron.* **11** 799
[18] Kang J U and Rodrigues A 2007 Fourier domain common-path fiber OCT with tunable reference: analysis and optimization *Quantum Electronics and Laser Science Conf.* JTuA55
[19] Vakhtin A B, Kane D J, Wood W R and Peterson K A 2003 Common-path interferometer for frequency-domain optical coherence tomography *Appl. Opt.* **42** 6953
[20] Tumlinson A R, Barton J K, Povazay B, Sattman H, Unterhuber A, Leitgeb R A and Drexler W 2006 Endoscope-tip interferometer for ultrahigh resolution frequency domain optical coherence tomography in mouse colon *Opt. Express* **14** 1878
[21] Park J S, Jeong M Y, Jung C H, Ouh C H, Kang H J, Han Y G, Lee S B and Kim C S 2010 Flexible curled optical cord for bending-insensitive optical imaging delivery *IEEE J. Sel. Top. Quantum Electron.* **16** 1031
[22] Joo C, Akkin T, Cense B, Park B H and de Boer J F Spectral-domain optical coherence phase microscopy for quantitative phase-contrast imaging *Opt. Lett.* **30** 2131
[23] Offroy M, Roggo Y, Milanfor P and Duponchel L 2010 Infrared chemical imaging: spatial resolution evaluation and super-resolution concept *Anal. Chim. Acta* **674** 220